



American Society of
Mechanical Engineers

ASME Accepted Manuscript Repository

Institutional Repository Cover Sheet

Cranfield Collection of E-Research - CERES

First

ASME Paper Title: A loss and deflection model for compressor blading and high negative incidence

Authors: Luis Ferrer-Vidal Espana-Heredia, Marc Schneider, Alessandro Allegretti, Vassilios Pachidis

ASME Journal Title: Journal of Turbomachinery

Volume/Issue: Vol. 141, Issue 12, December 2019
ASME Digital Collection

Date of Publication (VOR* Online): 25.9.2019

URL: <https://asmedigitalcollection.asme.org/turbomachinery/article/141/12/121001/975863/A-Loss-and-Deflection-Model-for-Compressor-Blading>

DOI: <https://doi.org/10.1115/1.4044967>

*VOR (version of record)

A loss & deflection model for compressor blading at high negative incidence

Luis E. Ferrer-Vidal*

Cranfield University, Bedfordshire, UK
l.ferrer-vidal@cranfield.ac.uk

Marc Schneider

Cranfield University, Bedfordshire, UK
marc.schneider@rwth-aachen.de

Alessandro Allegretti

Cranfield University, Bedfordshire, UK
alessandro.allegretti@cranfield.ac.uk

Vassilios Pachidis

Cranfield University, Bedfordshire, UK
v.pachidis@cranfield.ac.uk

Abstract

While significant advances have come about for turbomachinery off-design performance characterisation using computational fluid dynamics, the need for quick performance estimates at challenging off-design conditions still requires the use of lower-order models, such as mean-line analyses and through-flow tools. These inviscid tools require blade performance correlations formulated in terms of loss and turning angle as a function of blade geometric and aerodynamic parameters. Traditionally, such correlations have relied on empirical data from blade cascade tests at nominal incidence conditions. This limitation on the applicability of the blade correlations has caused performance modelling of the sub-idle regime to be off-limits to this type of correlation-based approaches. This paper addresses the development of blade loss and deviation models applicable to the sub-idle regime using a parametric numerical approach. 2D CFD results are used to generate a model that is then applied to mean-line and through-flow analyses aimed at predicting the sub-idle map of an axial flow compressor. The model proves to be a valuable tool for quick sub-idle performance estimates

and allows existing correlation-based performance prediction methods to be extended into the sub-idle regime.

1. Introduction

Operation below the idle speed subjects compressor blading to negative incidences far from the design point. As shown in Figure 1, during ground start on a machine with multiple spools, the cranked compressor will experience positive incidence in the front stages and run close to the stall line, however the rest of the compressors will be caused to windmill by the incoming airflow and will experience negative incidence. During steady windmilling after in-flight flameouts, all compressors will be subjected to negative incidence. The extent of negative incidence is especially severe for downstream stages, where the lack of compression coupled to a convergent flow path causes the axial velocity to increase while the rotor velocity remains relatively low, resulting in high flow coefficients with the subsequent drop in loading. Such off-design conditions are typically termed ‘sub-idle operation’ [1].

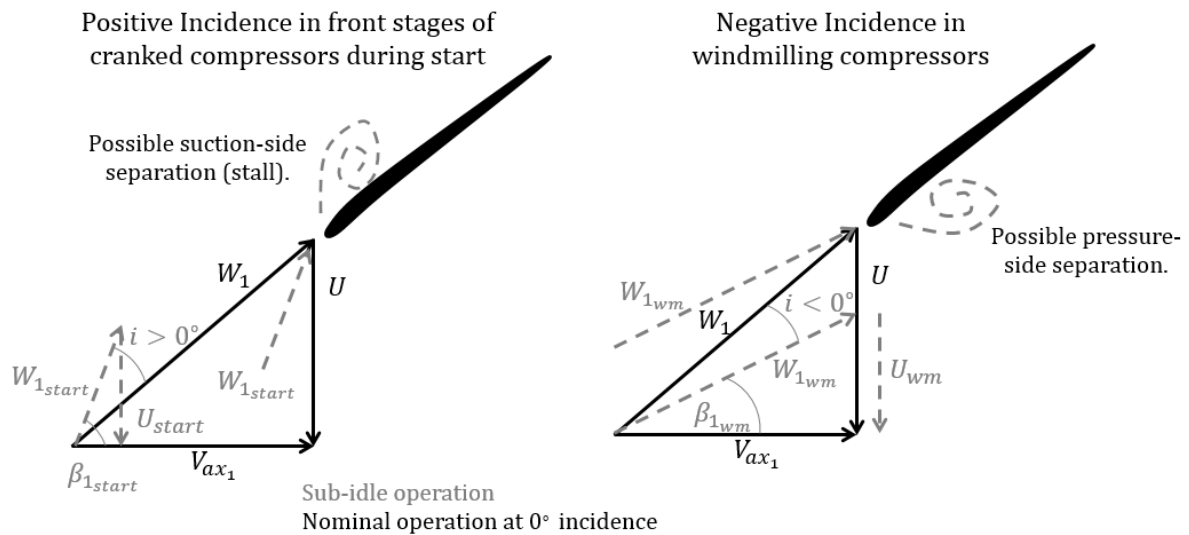


Figure 1: Incidences in compressors during sub-idle operation.

The drive for improved efficiency, short start times and increasingly stringent start and relight capability requirements, imposed by both the customer and the regulator, have rendered modelling of these sub-idle events an important aspect of engine development [2]. In order for these simulations to

be carried out, performance maps characterising engine component performance below the idle speed are required. A variety of methods may be employed to generate these maps during the engine design process before a rig is available. In the case of the axial flow compressor, through-flow tools and mean-line methods are typically used to solve the conservation equations in a reduced form, employing blade performance correlations in the form of loss coefficients and deviation angles to include viscous effects stemming from the presence of blade-rows.

For completeness, the definition of loss coefficient (ω), deviation angle (δ), deflection angle (ϵ), and incidence angle (i) as traditionally used in the correlation literature and in this study is as follows:

$$\omega = \frac{P_{t2} - P_{t2}}{P_{t1} - P_{s1}}, \quad \delta = \beta_2 - \kappa_2, \quad \epsilon = \beta_1 - \beta_2, \quad i = \beta_1 - \kappa_1 \quad (1)$$

Where (β) and (κ) are the flow and blade metal angles respectively. A summary of compressor loss mechanisms is given by Denton [3].

Correlation-based methods have typically been geared towards solving the design problem. The vast majority of correlations present in the literature have thus been developed for blades operating at or near nominal conditions. In the sub-idle regime, low shaft speeds and comparatively large mass flows result in high flow coefficients and associated negative incidences [4]. Negative incidences beyond -20° present at sub-idle makes existing correlations unsuitable. Lieblein [5] correlated blade loss to the diffusion factor, but those correlations were aimed at obtaining the minimum loss and associated incidence and deviation angles. Lieblein [6] also correlated blade loss coefficients with the boundary layer form factor, but this was only done for the attached flow case and thus not applicable to the negative incidences typically encountered during sub-idle operation. Similarly, Koch & Smith [7] produced loss correlations for design point conditions. In order to extend these design point correlations to off-design conditions, Cetin, Ucer, Hirsch and Serovy [8] included a correction based on the $(i - i_{ml})$ parameter, which ties off-design incidence to that of minimum loss for a given blade, but the lowest incidence studied corresponded to a $(i - i_{ml})$ value of -7 degrees. Howell's correlations from 1945 [9] notably extend considerably into the negative incidence range, with up to -20° considered, but do not

cover the range expected for sub-idle conditions, which can exceed this value. For deviation angle, the most widely known correlation is that of Carter[10], which correlates the design deviation angle with blade solidity, camber and stagger. For off-design incidences, Creveling and Carmody [11] correlated deviation data to incidence referenced to minimum loss, but their data is again focused on off-design positive incidences. Most recently [12], attempts at predicting the windmilling performance of axial compressors have looked at using Aungier's [13] correlations at negative incidence, but this required the extrapolation of those analytical functions to incidences not meant for their application, requiring adjustments to obtain physical values.

A need exists for blade performance correlations for negative incidence. In order to make correlation-based methods applicable to the sub-idle region and to allow for calculation of compressor characteristics below the idle speed, this investigation looks at using steady state computational fluid dynamics to obtain loss and deviation trends of compressor blades subjected to high negative incidences. This data is reduced to models that can then easily be applied to established compressor analysis methods.

2. Methodology

A 2D parametric model is set up in ANSYS Workbench with FLUENT as the flow solver. This allows the model to take full advantage of the parametrization available within the ANSYS Workbench environment. A blade profile representative of a modern core compressor is used. Boundary conditions used include a total pressure inlet, allowing velocity components to be specified, and a static pressure outlet with a mass-flow target. Periodic boundaries are used to form the cascade as shown in Figure 2. No-slip wall boundary conditions are used on the blade geometry. A full sweep of incidence angles is performed by setting the pressure inlet boundary condition velocity components. The solidity and stagger are controlled via parametric controls on the geometry model that trigger an automatic update on the model mesh. Solidity is controlled by varying the pitch between blades, while the stagger is implemented as a simple rotation on the modelled profile. A baseline model is first obtained using an

incompressible model. Compressible models are then run to obtain a correction based on Mach number. This is done to separate the effects of cascade geometry from compressibility effects, as varying cascade stagger and solidity as part of a parametric sweep results in varying inlet Mach numbers. For compressible simulations, the inlet Mach number is controlled via the outlet mass flow target boundary condition, such that it can be kept within a certain pre-determined range. Reynolds number can be adjusted via the total pressure inlet boundary. The Sutherland law is used to model viscosity as function of temperature and calorically perfect air is assumed with an adiabatic coefficient of 1.4. The simulations are steady state RANS with a k- ω SST turbulence model. This model is chosen for its proven performance in wall-bounded flows, low wall-resolution requirements, and limited eddy viscosity production in re-circulation regions. The applicability of steady RANS models to the expected separated flow is not considered in the study, but justification for their use is made on the grounds of needing to establish trends from multiple simulations and the proven performance of the model within low-order tools.

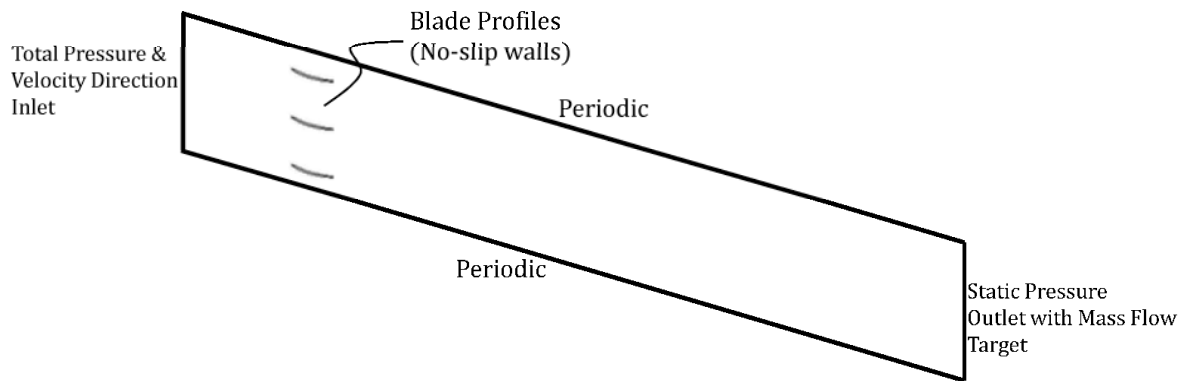


Figure 2: Model domain.

The ANSYS meshing software was used to generate the mesh. This software allows for generation of un-structured grids with inflation layers. Three meshes with a uniform refinement ratio of two were used in complete incidence angle sweeps at a stagger of 45° and solidity of 1.2. Figure 3 shows the fine-grid Grid Convergence Index (GCI) [14] of the selected mesh for the negative incidence range, calculated with a safety factor of 1.25. The large GCI for pressure loss coefficient towards low negative

incidence is due to the low losses in that region magnifying the relative error; hence, absolute error for loss coefficient and deviation angle is also shown (ω_d, δ_d). In terms of an averaged value over the range, both parameters result in a GCI < 5 %. This is considered adequate for this study. The medium mesh was selected based on its equivalent results compared to the fine mesh and the need for quick turnaround in the development of a blade performance database. For the selected mesh, a wall resolved mesh was used with y-plus values below two, expansion ratio limited to 1.2, and 20 inflation layers, to ensure proper boundary layer resolution [15].

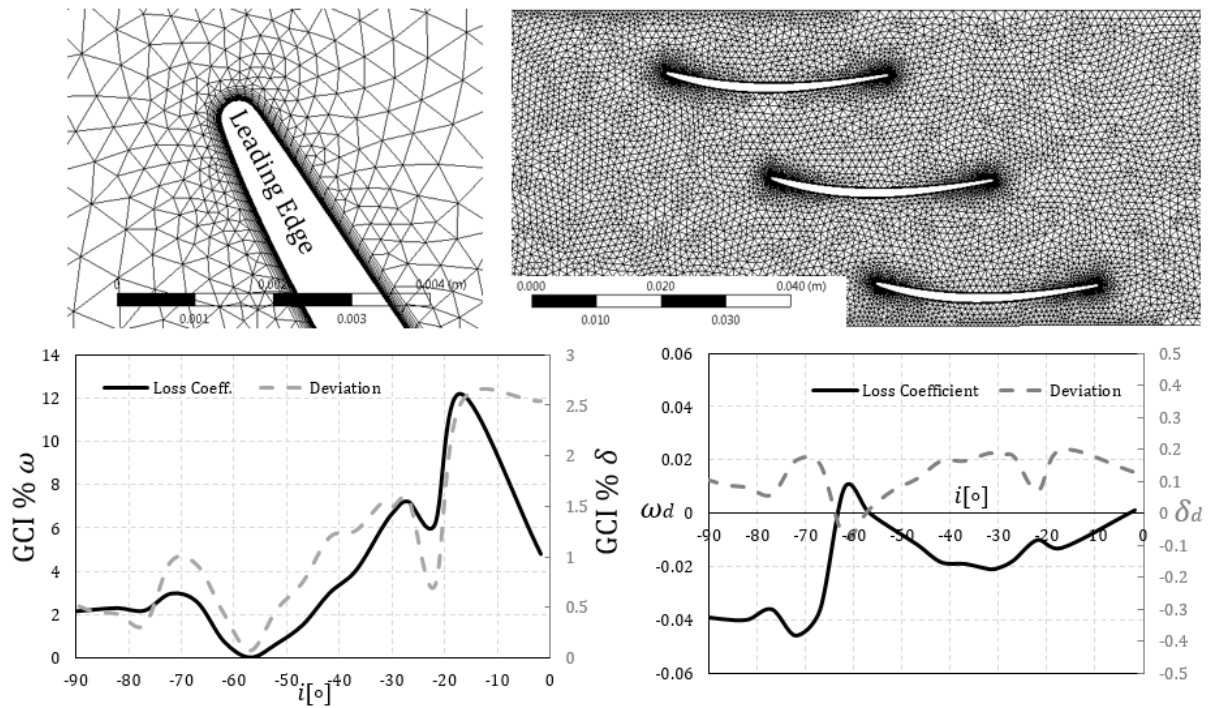


Figure 3: Mesh sensitivity study results (bottom) and close-up of mesh used (top).

Total pressure and flow angle measurements are taken at the outlet plane. As shown in Figure 4, a stable measurement of mass-flow averaged blade exit flow angle is achieved after a distance of 5 blade chord lengths from the blade trailing edge. This study was done for a single case at an incidence of -65°, stagger of 45° and a solidity of 1.2, resulting in a largely separated flow field. Consequently, the domain outlet and reading location for all cases has been set at 13 chords downstream of the trailing edge ensuring the flow field has had enough distance to reach a representative mixed-out state. The choice of a single set of thermodynamic properties to represent the separated flows occurring at negative

incidence is not a trivial problem, and the choice of the averaging procedure needs to be selected concerning the application [16]. The choice of using the mixed out condition is made not only due to practical concerns, but also because it is considered the most appropriate option for use of the model within low-order tools that do not account for transport of flow non-uniformity. The mixed out state accounts for all the entropy generated due to mixing, even if this occurs downstream [17]. While the presence of a downstream blade-row would have an upstream influence, this is not modelled based on trying to obtain the mixed-out solution for the effects of a single blade-row. This approach is deemed appropriate considering the targeted application, since low-order compressor models would typically employ some form of mixing assumption between blade-rows, as is also commonly done for steady-state turbomachinery CFD [18]. It would be possible to obtain a form of correlation for blade deviation angle vs. spacing, but the authors have found this difficult to correlate for a wide range of geometry settings. The mixed-wake assumption can be considered an adequate compromise for windmilling cases, where the relative rotation of components would enhance mixing, but can be expected to decrease in applicability as the shaft speed reduces to zero.

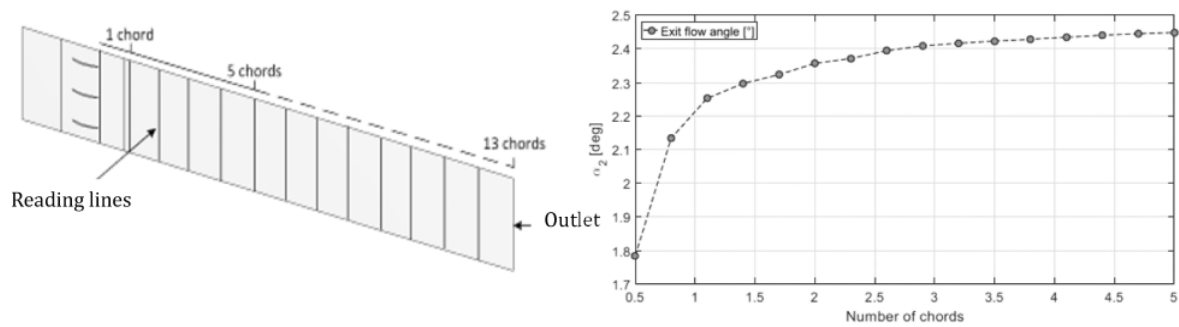


Figure 4: Impact of reading location on result [19].

Model development

In order to obtain a generic and useful model, a range of negative incidences, solidity, staggers, and Mach numbers is investigated. Incidence is considered the dominant parameter, as it sets the blade velocity triangles. Solidity and stagger are included in the model as these set the passage geometry. Solidity quantifies the non-dimensional width of the passage (blade pitch) available to channel the flow

[20]. Similarly, stagger establishes the passage length that is available to guide the flow. The effect of stagger on the guided flow area is illustrated in Figure 5. While blade camber sets the amount of flow turning near nominal conditions, it has not been included in this model. The justification for this is that the separated flow fields present at high negative incidence dominate over the effects of blade shape [21]. Mach number is included to account for compressibility effects as the passage approaches the choking condition.

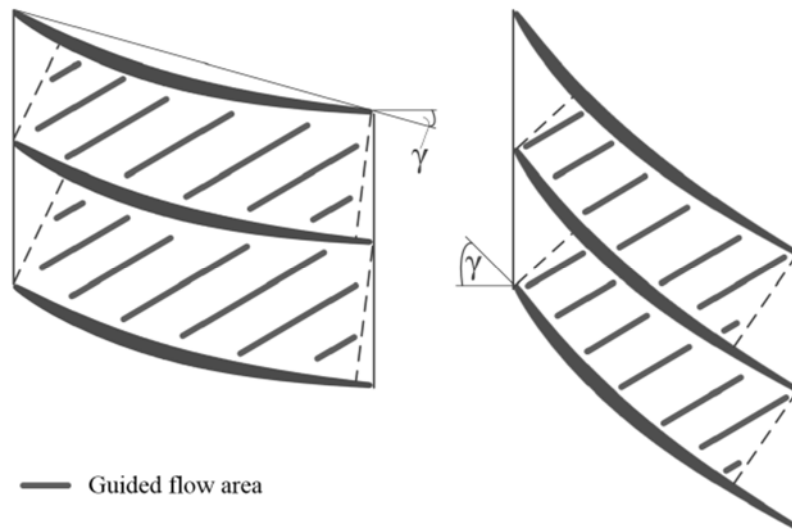


Figure 5: Effect of stagger on guided flow area [22].

Full incidence sweeps at each solidity & stagger combination are performed from -90 to $+20$ degrees. Six values of solidity from 0.5 to 2.5 and four values of stagger from 15 to 55 degrees are considered. This range is selected based on typical compressor design scenarios [23]. With this baseline model at hand, the effects of Reynolds and Mach number are considered by employing only a single solidity & stagger combination in order to develop an appropriate correction. Overall, 576 CFD simulations are used in a full factorial scheme to obtain the baseline model as a function of incidence, stagger and solidity. The results are curve fitted with smoothing splines and re-sampled to obtain tabular data at equally spaced intervals. This allows the data to be used within efficient interpolation routines. Table 1 shows the parameter range used to create the model. For the study of Mach number effects, four different outlet mass flows are imposed to obtain four different Mach number levels in full incidence sweeps at a single solidity and stagger. While the incidence range of -90° to $+20^\circ$ was studied

in 5° increments, further sub-divisions were tried in certain cases to acquire a good resolution of the trend.

Table 1: Parameter space for model.

Incidence (i)	Solidity (σ)	Stagger (γ)
$-90^\circ : +20^\circ$	0.5, 0.7, 1.0, 1.5, 2.0, 2.5	15, 30, 45, 55

Model Assumptions

A number of simplifying assumptions have been made to develop the model. A single blade profile has been used considering the notion that, due to the separated wakes dominating the flow-field for high negative incidence, the effects of blade camber and thickness distribution (i.e. blade shape) will be of second order when compared to those of passage geometry [21]. Studies with differently profiles could be used to establish an additional correction for camber and thickness effects, but this is out of the scope of this paper. Additionally, it must be noted that the 2D model implementation does not allow for the effects of AVDR (Axial Velocity-Density Ratio) to be investigated; i.e. AVDR is taken as unity for all cases investigated in this work. From 3D numerical simulations, the authors have observed AVDR values for windmilling compressors tending above unity but always below 1.2, signalling that the flow can still be considered quasi-dimensional [24]. The low loading (low compression) and converging geometries are responsible for the AVDR being driven up at sub-idle. A correction for AVDR effects specially geared towards high-negative incidences along with corrections for the effects of induced flows, as has been done for similar studies [25], would be notable additions. This has however remained outside the scope of this study.

3. Results

The data gathered is first analysed to understand the trends in deviation angle and guide the development of the final model. The base-line model based on the parameters of incidence, stagger and solidity are then introduced. Finally, corrections for Reynolds and Mach number are discussed.

Deviation angle trends

During the preliminary studies, it was observed that deviation angle measurements did not follow a smooth or monotonic trend, making analytical representation and interpolation difficult. After further study, it was concluded that all deviation vs. incidence angle trends, at all solidity and stagger combinations could be described by a similar shape. Such a shape is characterized by two sections separated by a clear discontinuity or “kink” in the overall trend. This point was seen to correlate with the point at which the separated flow bubble, present on the pressure side of the blade, is no longer able to re-attach. This point is named the “full-detachment” point by the authors. Beyond this negative incidence angle, the deviation angle trend is seen to either decrease sharply for low solidities (below 1) or to slightly increase and reach an almost constant value at high solidities. For all cases, the deviation trend at lower negative incidence angles follows the expected bucket shape [13]. A representation of a typical deviation angle trend is shown in Figure 6 identifying the zero-lift and boundary layer full-detachment incidences for a modern blade. As the incidence becomes negative, the boundary layer (BL) separates from the leading edge and re-attaches before the trailing edge on the pressure side, creating a re-circulating flow bubble. At a certain point, the lift generated by the blade becomes null (zero-lift incidence) as the BL re-attachment moves closer to the trailing edge. Shortly after the zero-lift incidence, the BL is no longer able to re-attach, and a large wake region of separated flow is created, affecting the deviation angle trend.

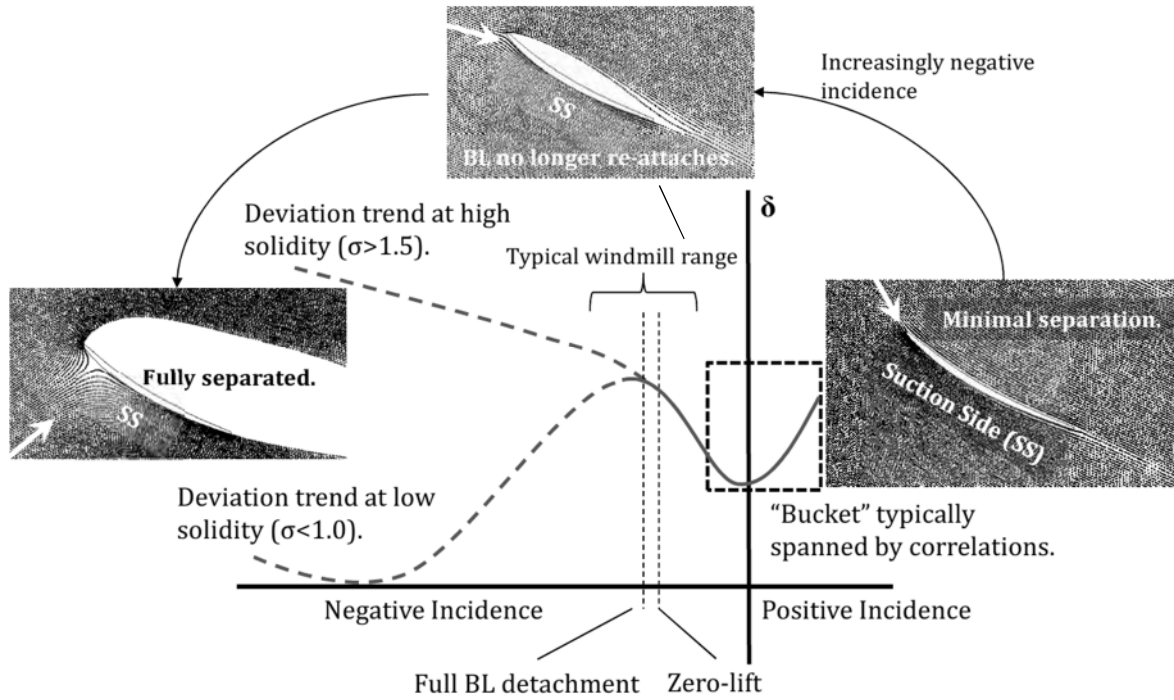


Figure 6: Typical deviation trend with increasingly negative incidence for a modern compressor profile.

The position of this full-detachment incidence could be used as a dividing point to separate two different trends from which to fit an analytical model. Such an approach was initially tried with decent results. However, it was found that slight discontinuities due to separate curve-fits at the boundary between the trends to the left and right of the full-detachment incidence could result in unrealistic sub-idle characteristics being calculated when used within a through flow code. After further analysis, it was found that the trend for deflection angle follows a smoother trend, allowing easier use of interpolation routines or as a means to generate an approximate analytical model. Therefore, the model developed in this investigation has been generated in terms of loss and deflection angle. This deflection angle can then easily be converted to a blade deviation angle with knowledge of the blade geometry or the knowledge of a reference deviation angle at a specified incidence. A plot of a deviation angle trend along with the corresponding trend in deflection angle is shown in Figure 7. The deviation angle trend can be obtained from the deflection angle via the following relationship assuming an inlet metal angle of 0° :

$$\delta = i - \epsilon + \epsilon_{ref} + \delta_{ref} \quad (2)$$

Using this relationship and an assumed $\delta_{ref} = 0^\circ$ at 0° incidence, deviation angle plots can be obtained in terms of a $\Delta\delta$ referred to 0° incidence. It should be noted that the difference in the full-detachment deviation angle with solidity for blades of the same stagger shown in Figure 7 is a direct result of the $\Delta\delta$ formulation and the deflection model; making this a function of the reference deviation as well. The position of the full-detachment incidence is seen to occur a few degrees after the zero-deflection incidence angle, which may also be described as the zero-torque or zero-lift incidence angle. As expected for such highly cambered modern aerofoils, the zero-lift incidence occurs at a moderate negative incidence, in the order of -20° . Blades of the same stagger are seen to reach the no deflection condition at approximately the same incidence angle regardless of solidity, suggesting the zero-lift condition is only a weak function of this parameter.

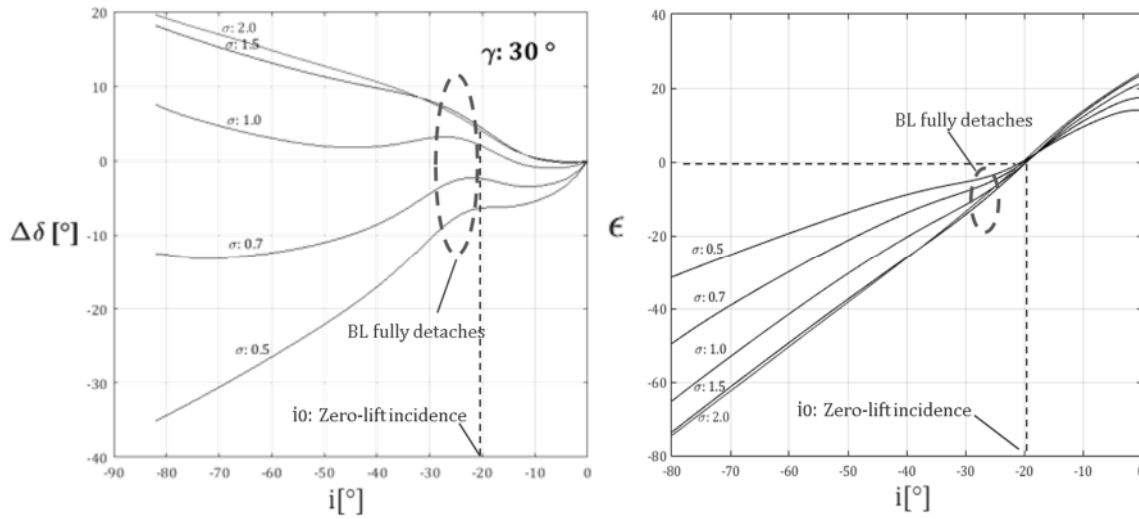


Figure 7: Deviation (left) & deflection (right) vs incidence angle trends, with the relative location of the full-detachment and zero-lift incidence angles.

The zero-lift, or zero-deflection, incidence angle is considered an important blade-performance parameter when dealing with sub-idle operation, as it signifies the incidence angle at which a particular blade profile will achieve torque-free operation. In this sense, a rotor comprised of a prismatic blade element (i.e. extruded constant profile) would be expected to achieve a steady-state torque-free windmilling speed such that the incidence angle on the blade profile corresponds to that of zero lift.

More generally, the zero-lift incidence marks the incidence angle at which a particular profile is no longer able to add enthalpy to the flow, thermodynamically acting like a turbine for incidence angles below the zero-lift incidence.

Base-line model for loss & deflection

As discussed, the obtained CFD points are curve fitted with smoothing splines and re-sampled to generate a model for a range of incidence angles spanning -90° to 20° . As points near the extremes were not numerically obtained for all cases and few points were gathered in the positive incidence range, the final model is only presented for incidences between -80° and 0° , ensuring the model is well within the bounds of the data collected. The model is shown for staggers of 15° to 55° in Figure 8 to Figure 11. While values solidity values up to 2.5 were considered, all deflection angle trends collapse onto a single trend for solidities beyond 1.5. For clarity and to aid implementation, only solidities up to 2 are shown in the deflection data. These may be considered to apply as limiting values for $\sigma \geq 2$.

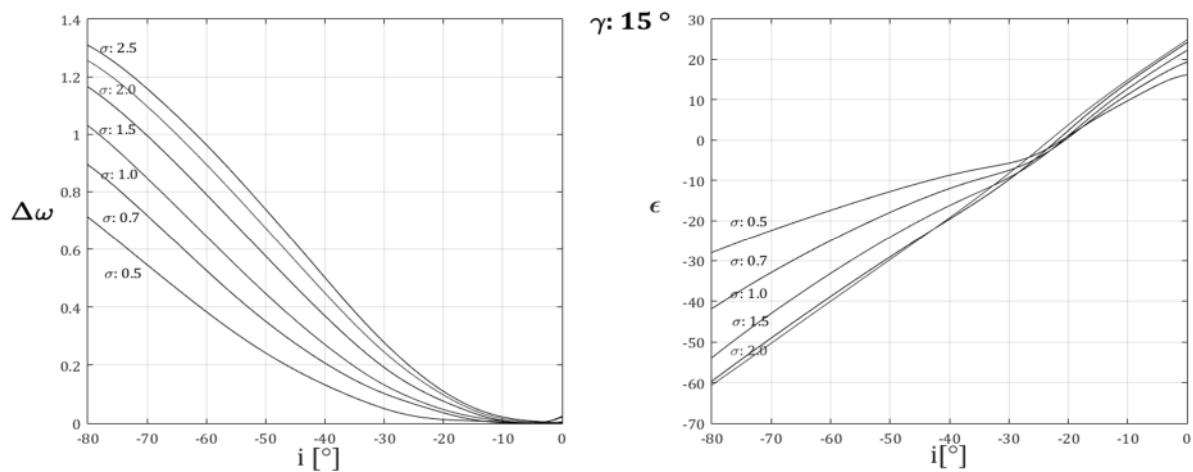


Figure 8: Loss coefficient and deflection angle at negative incidence for 15° stagger.

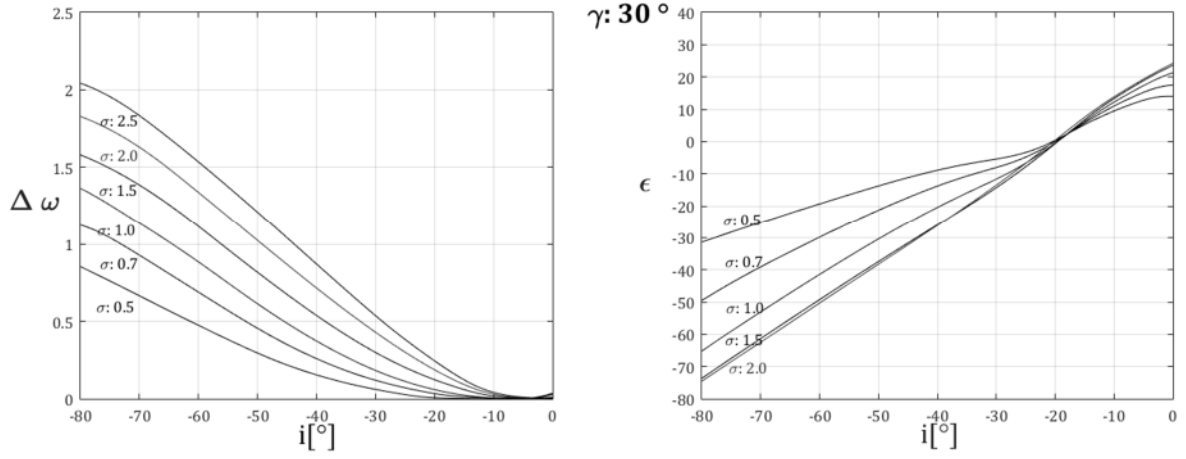


Figure 9: Loss coefficient and deflection angle at negative incidence for 30° stagger.

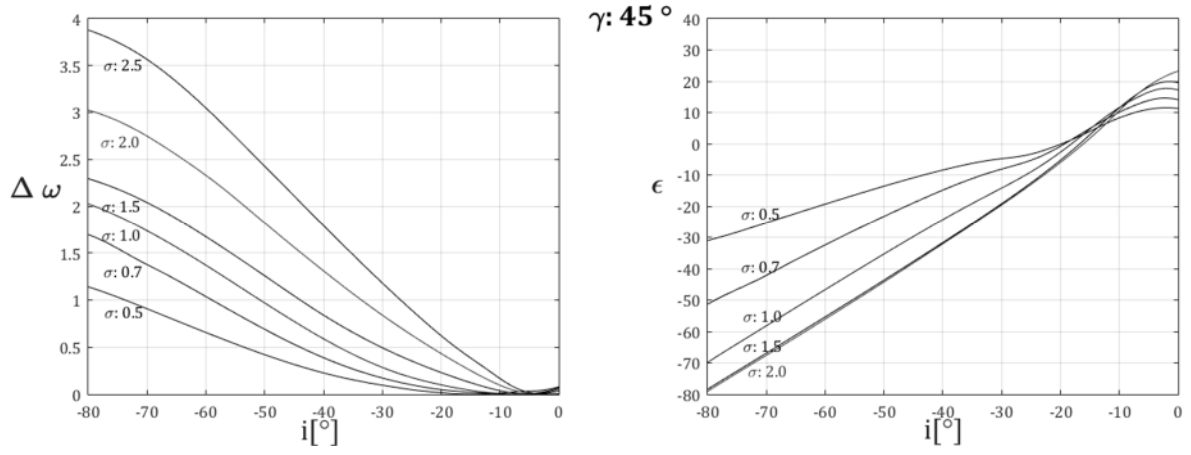


Figure 10: Loss coefficient and deflection angle at negative incidence for 45° stagger.

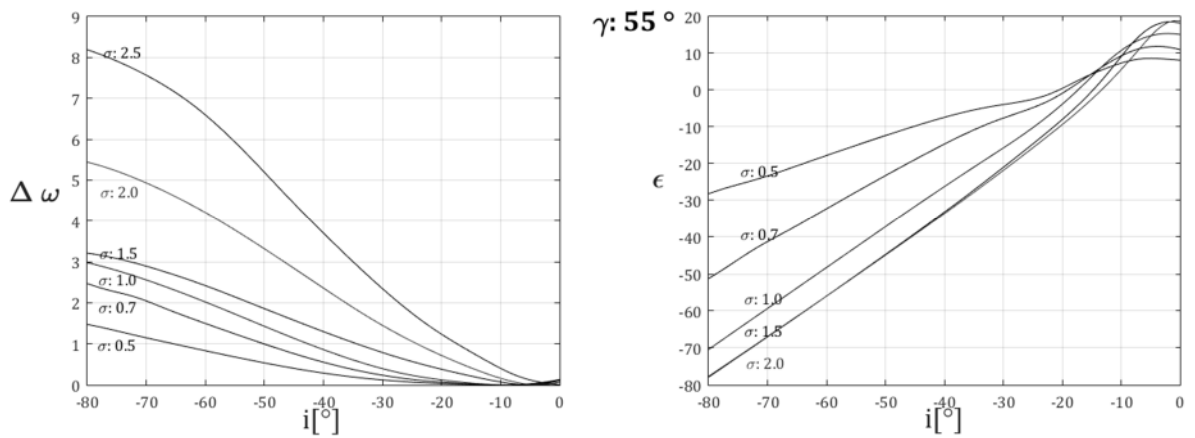


Figure 11: Loss coefficient and deflection angle at negative incidence for 55° stagger.

The loss coefficient data is presented in terms of a $\Delta \omega$ value, which is referenced to the minimum loss coefficient obtained in the study. Therefore, any implementation of the presented model requires prior knowledge of the blade minimum loss. For the blade studied, the minimum loss incidence angle was found to lie in the range of $-7^\circ:0^\circ$ for all cases studied, with a very flat low-loss bucket. The zero-lift (zero-deflection) incidence angle for this blade occurred for all cases in the range of $-23^\circ:-19^\circ$. The data is presented here in terms of a raw incidence angle to allow the most convenient non-dimensional incidence parameter to be used for the given application.

The incidence parameter could be normalized by taking into account the specific blade's minimum loss and zero loss incidence as shown in Equation (3). Such a parameter describes the incidence angle as a function of the range to the zero lift incidence, in a similar manner to the incidence parameter used by Aungier [13]. This parameter may be used to adapt this model to blades of different camber. An important matter to keep in mind when using such a parameter with wildly different profiles is the unrealistic stretching of the graphs which may occur for profiles with zero-lift incidences much closer to that of minimum loss.

$$i' = \frac{i - i_{ml}}{i_0 - i_{ml}} \quad (3)$$

In addition to the presented deflection data, deviation angle trends may be obtained using Equation (1). These are shown in Figure 12.

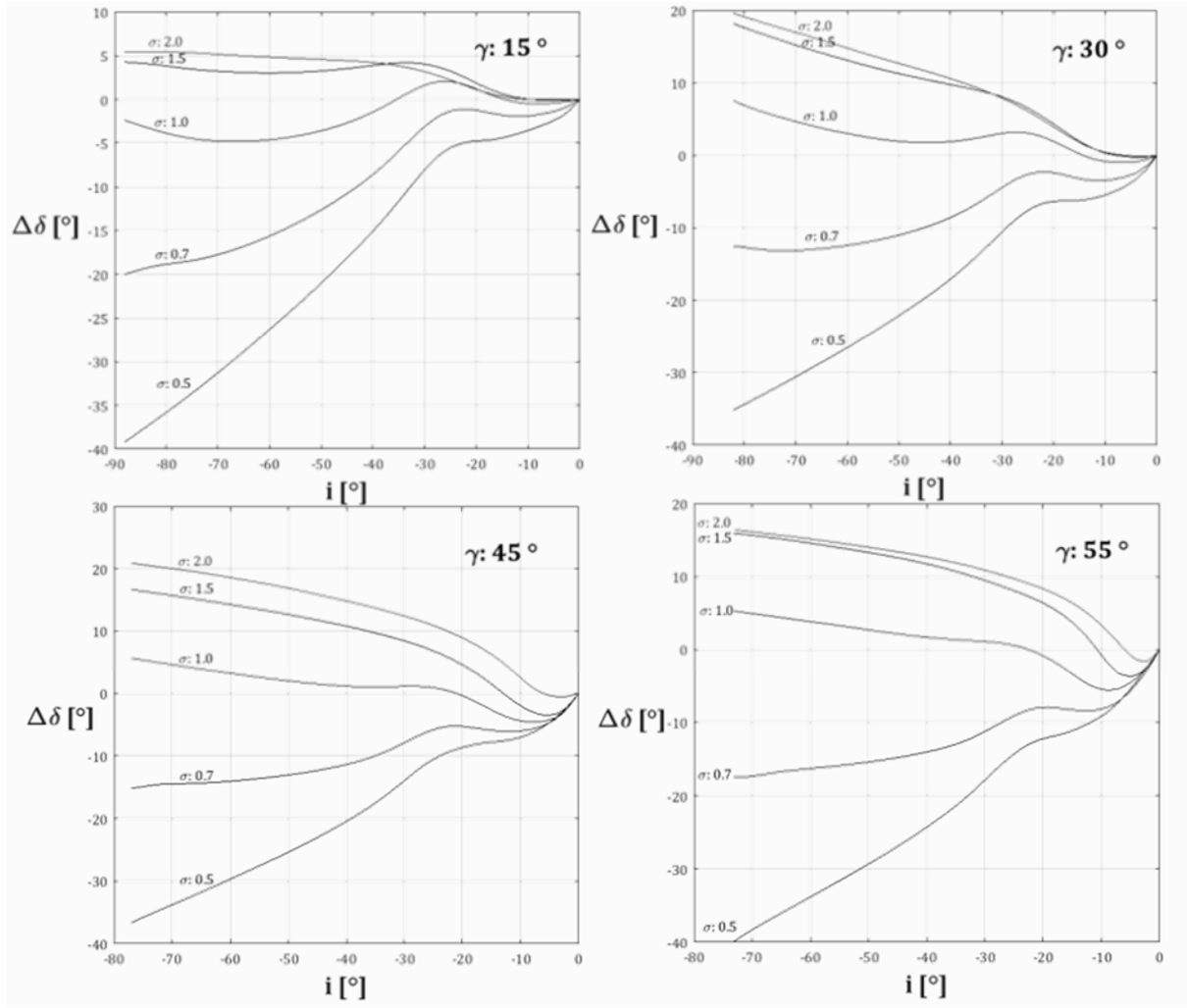


Figure 12: Deviation angle trends obtained from deflection model.

Reynolds and Mach effects

In addition to the model based on solidity, incidence, and stagger, corrections to account for the effect of Mach and Reynolds may be desired. The effect of Reynolds number in the range 1E4 to 5E5 is first assessed by performing full incidence sweeps at a single setting of stagger and solidity. The range of Reynolds numbers studied is based on values observed in 3D numerical studies done in parallel to this study, but lower values could potentially exist and this is a model limitation. No discernible differences are seen on the deviation angle trend over a range of Reynolds ranging from 1E4 to 5E5, with only slight changes in the loss coefficient seen for $Re < 1E4$. As a result, the effect of Reynolds number has not been considered for this model in the interest of simplicity. The model developed within this work can be considered valid without Reynolds corrections when operating at $Re > 1E4$.

It is important to note that the Reynolds study has been performed with fully turbulent RANS, so laminar effects cannot be studied. A transition model could potentially be used to study the possibility of locally laminar flow affecting flow separation around the leading edge, though such a study would perhaps require validation and calibration of the transition model itself. Correlation based approaches to study transition, such as those implemented by the MISES code, might also be worthwhile [26]. This has been previously used to study the effect of transition near leading edges and their effects on blade performance [27]. Such work is however out of the scope of this study. While locally laminar flow could potentially affect the deflection trends to some degree, these are likely to be dominated by the down-stream re-attachment rather than leading edge phenomena. These effects need to be further investigated however.

The effect of Mach number is seen to have a very noticeable effect on the loss coefficient. Cases at incidence settings of -18° and -62° are run at three different ratios of inlet Mach number to choking Mach, which measures how close the passage is to choking conditions. This initial study is done to qualitatively gauge the impact of Mach number on losses. The effects of Mach number on the loss coefficient are seen to follow a similar trend to that reported by Lieblein [28] as shown in Figure 13. As a result, a correction for loss and deviation angle as a function of the inlet to choking Mach number ratio into the blade passage is created. The philosophy behind the Mach number correction is to account for the physical trends rather than develop a detailed model, so a simple approach is adopted. Following the work of Horlock[29], there was an attempt to create separate correlations for critical inlet Mach (inlet Mach number for which supersonic flow first appears in the passage) to choking Mach (when the passage finally chokes). However, the small difference observed between the two led to the correction being formulated solely in terms of the choking Mach number.

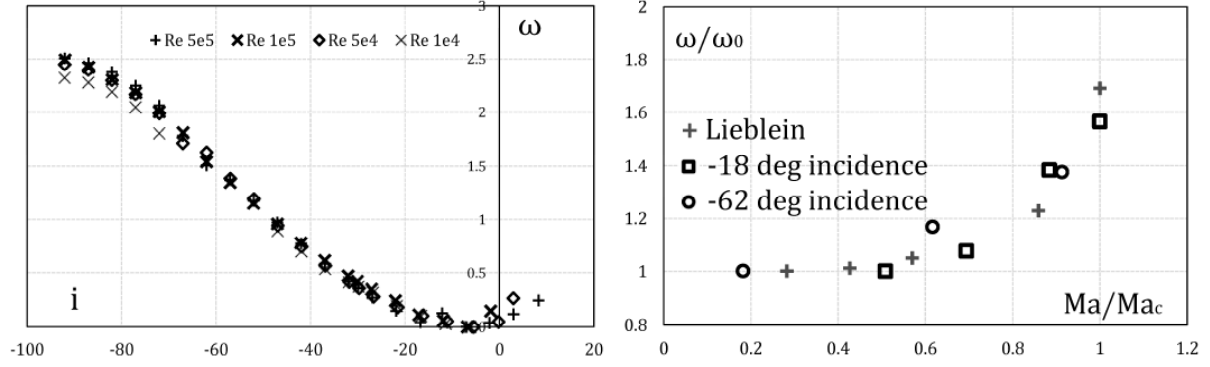


Figure 13: Effect of Reynolds number (left) and Mach number (right) on the loss coefficient measured.

Rather than performing full parametric sweeps with varying Mach number in addition to incidence, solidity and stagger, some simplifying assumptions are made. Namely, that the correction to the baseline model will be the same for a given ratio of inlet Mach to choking Mach, and that this ratio varies in the same manner with respect to incidence for all stagger-solidity combinations. The choking Mach number is the inlet Mach number for which the passage chokes. The Mach number correction is formulated in terms of three different correlations obtained from numerical results:

1. A correlation for choking Mach number vs. solidity and stagger at minimum loss incidence.
2. A correlation for the variation of choking Mach number vs. incidence.
3. Corrections to baseline loss & deflection based on the inlet to choking Mach ratio and incidence angle.

While the minimum loss incidence occurs at -2° for the case studied, 0° maybe taken as the reference point without noticeable effects on results. The first two correlations for choking Mach are shown in Figure 14, The effects of loss and deflection are shown in Figure 15, where $M/M_c = 0$ corresponds to the result from the incompressible model. Functional expressions for the correlations in Figure 14 are given in equations (4) and (5). The limited effect of Mach number on deflection angle can be accounted for via expression (6). For the loss coefficient, Figure 16 provides the change in loss coefficient in the form of a loss adder respect to the incompressible solution. Values may be interpolated from Figure 16 where the adder can be considered constant for incidences below -60° . Existing correlations (such as Lieblein's [28]) may be used for less negative incidences above -10° if required.

These corrections have not been developed to account for shocks, and so it is recommended to take $M/M_c = 0.8$ as the limiting value spanned by this correction, bounding inlet conditions and corresponding losses to this value.

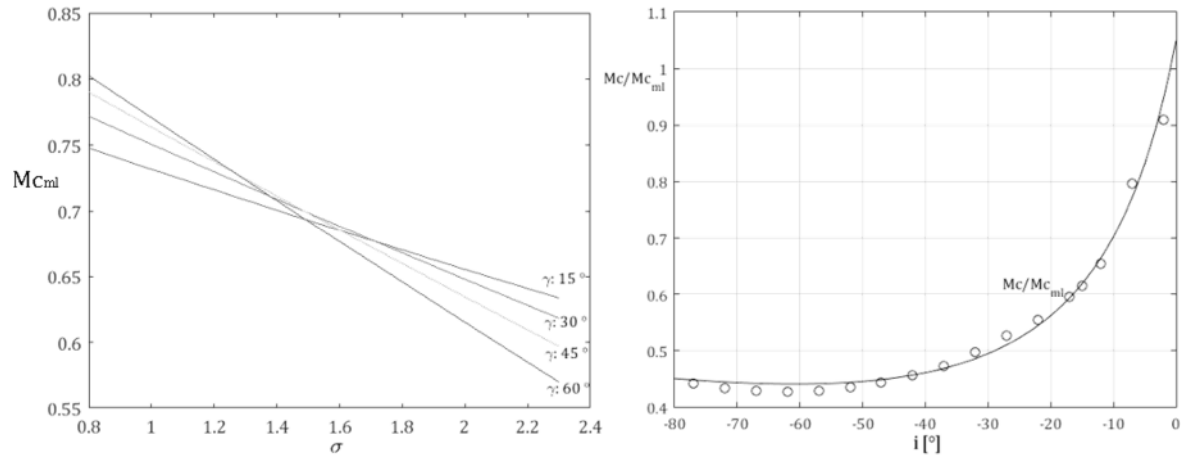


Figure 14: Choking Mach number at minimum loss incidence as a function of solidity and stagger (left). Choking Mach number correction for increasing negative incidence (right).

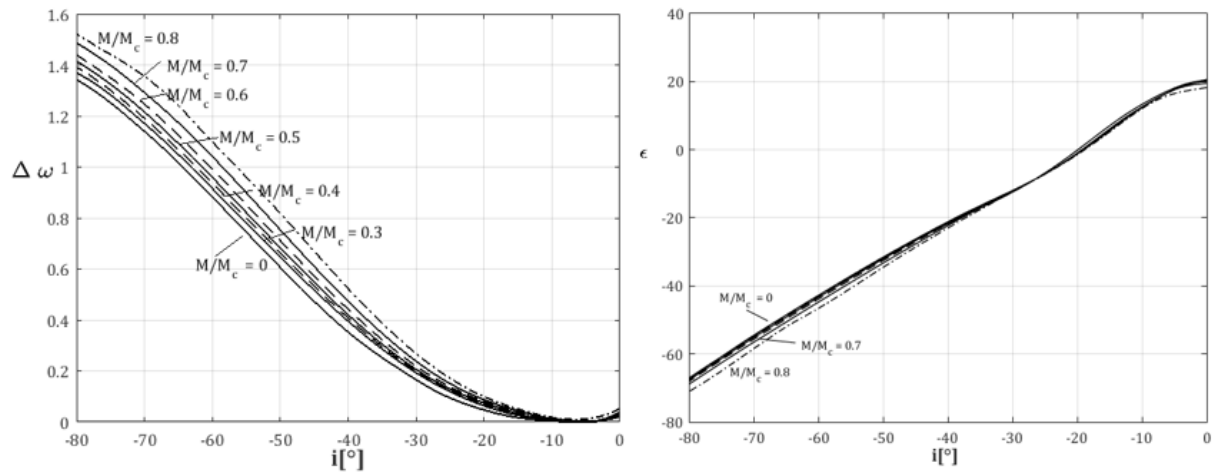


Figure 15: Loss correction vs incidence angle for different ratios of inlet Mach to choking Mach at solidity of 1 and 30° stagger.

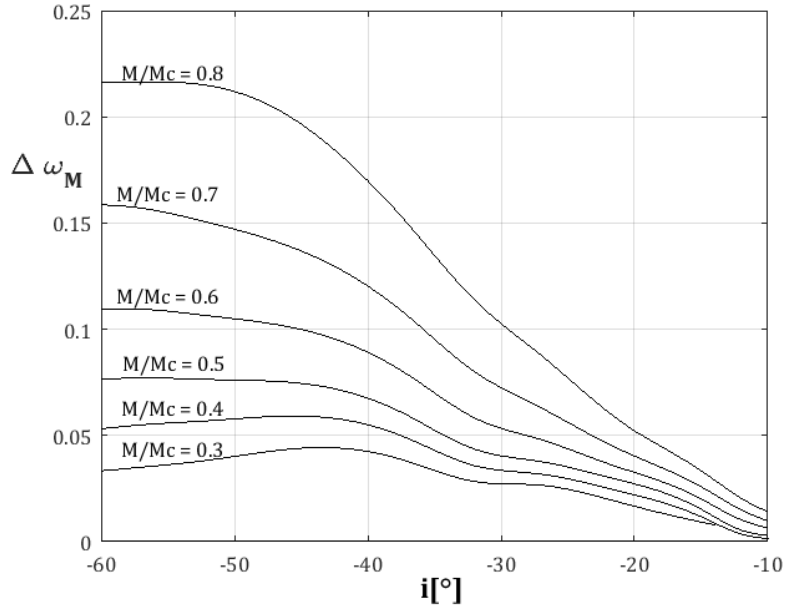


Figure 16: Loss coefficient adder due to inlet Mach number at different negative incidences.

$$Mc_{ml} = (0.7625 - (5.853 \times 10^{-2})\sigma + (2.891 \times 10^{-3})\sigma^2 - (1.759 \times 10^{-3})\sigma\gamma + (3.608 \times 10^{-3})\gamma - (1.31 \times 10^{-5})\gamma^2) \quad (4)$$

$$\frac{Mc}{Mc_{ml}} = \frac{7.391 \times i^2 - 317.8 \times i + 44300}{i^2 - 2368 \times i + 42220} \quad (5)$$

$$\Delta\epsilon_M = (-3.25 + 0.06 \times i) \times \left(\frac{M}{Mc}\right)^2 \quad (6)$$

Model Fitting

This negative incidence model has been developed to allow the calculation of compressor characteristics in the sub-idle regime. In order to make the model data useful to a mean-line or through-flow tool, the data must be load-able into a computer code. As analytical functions accurately capturing the trends seen here prove impractical, two different means to load this data into analysis codes have

been attempted: interpolation of tabulated data and the use of neural networks. The development of a neural network to yield both the loss and deflection angles was seen as a way to quickly reduce data into useful models [30]. The neural networks obtained consist of two hidden layers with eight neurons each. The Levenberg-Marquart learning algorithm with Bayesian regularisation was used for training. Concerns with Neural Network performance at the extremes of the parameter space also led to development of efficient interpolation routines. Ultimately, both an efficient interpolation routine and the neural network approach have been made available within the tools used. With its implementation consisting of matrix multiplication of the neural network weights, the neural network approach presents a considerable speed advantage when used within matrix manipulation codes such as Matlab, though care must be taken in using Neural Networks at extremes of the parameter space where fewer data is available for training. Figure 17 shows the loss and deviation models generated by both methods at a stagger angle of 45° for a wide range of solidities from 0.5 to 2.0. It is seen that over-fitting of the neural network has been avoided for the range of interest and that results of both methods are almost identical. However, it must be pointed out that if the Neural Network is used to retrieve values beyond the range of the parameter studied, the results will not be reliable. On the other, the interpolation will be satisfactory with any number of inputs. It is therefore important to bound input values to the underlying training data when using the Neural Network fit.

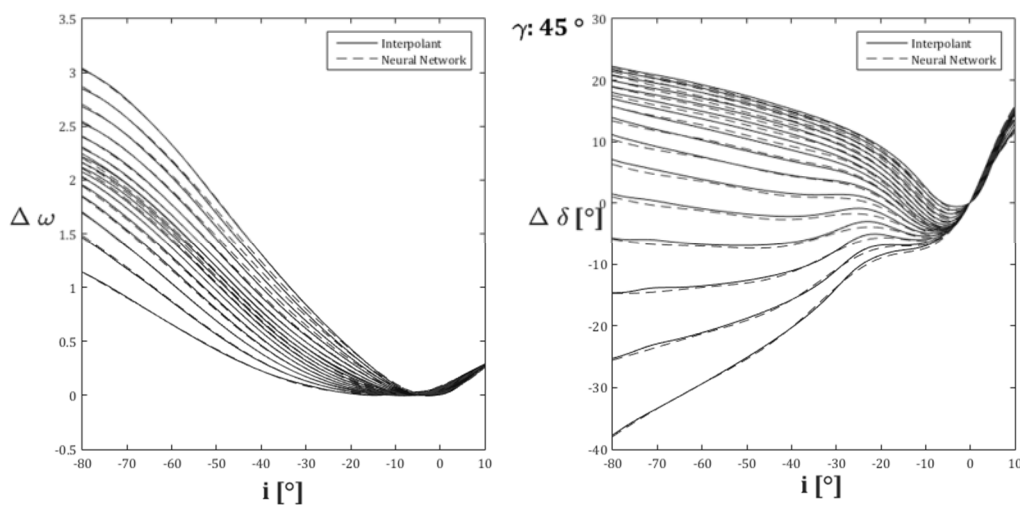


Figure 17: Neural network vs. interpolation output for 45° stagger and solidity range 0.5 to 2.0.

Table 2 shows the resulting root mean square error (RMSE) against underlying data for both approaches, calculated taking into account the entire negative incidence, stagger, and solidity range. Table 3 shows the maximum error for the same range along with the respective location. For all cases except the deflection Neural Network, the maximum error occurs at high stagger and positive incidence. In the whole, both approaches perform equally for the loss coefficient while the interpolation performs better for deflection angle. While errors on loss coefficient appear large compared to design values, these are due to larger absolute errors at high negative incidence which are small in relative terms. The maximum loss coefficient errors quoted below correspond to $\sim 3\%$ relative error.

Table 2: Root mean square error of fit with underlying data for the Neural Network and Interpolant functions.

	RMSE Neural Network	RMSE Interpolant
Loss coefficient (ω)	0.0383	0.0383
Deflection (ϕ)	0.3412	0.1419

Table 3: Maximum error of fit with underlying data for the Neural Network and Interpolant functions.

	Max. Error Neural Network	Max. Error Interpolant
Loss coefficient (ω)	0.1329 ($\sigma = 2, \gamma = 55^\circ, i = -67^\circ$)	0.1304 ($\sigma = 2, \gamma = 55^\circ, i = -82^\circ$)
Deflection (ϕ)	2.0334 ($\sigma = 2, \gamma = 15^\circ, i = -7^\circ$)	1.771 ($\sigma = 2, \gamma = 55^\circ, i = -2^\circ$)

Application

The results of using the model within ACROSS (Axial Compressor Rotating Stall and Surge), a 3D Euler code [31], and a 1D mean-line tool are shown and compared against 3D CFD and experiment in Figure 18 and Figure 19. Both ACROSS and the 1-D mean-line code make use of the model developed in this work. The comparison between the two allows an assessment of the model's implementation within a mean-line representation of the geometry and a higher-fidelity approach that considers the spanwise variation in the blading. The mean-line code includes the Pollard & Gostelow correction for AVDR effects on deviation angle [32]. For these cases, a six stage axial compressor from an Allison

M250 turboshaft is modelled. Experimental data is available in the form of a locked rotor characteristic, where the compressor is not rotating and an axial flow is imposed, and a windmilling line, where an axial flow is imposed and the compressor is allowed to windmill freely. For the locked rotor case, Figure 18 shows pressure ratio and torque, as the enthalpy parameter is not defined in the sub-idle range [33] [34]. For the windmill case, Figure 19 shows the relationship between windmill speed and mass flow instead of the torque map, as this is assumed negligible in the windmill condition. Further discussion on the use of this model within an Euler code and its implementation in modelling sub-idle characteristics can be found in [35]. As seen for this specific geometry, the implementation of the blade model in a mean-line approach differs only slightly from the spanwise application of the same model in ACroSS. The matching compares well against RANS CFD as only bulk performance parameters are compared. Even with the new model, the mean-line approach would be expected to underperform RANS CFD as choke is approached, and a slight divergence to this effect is observed in the calculated characteristics.

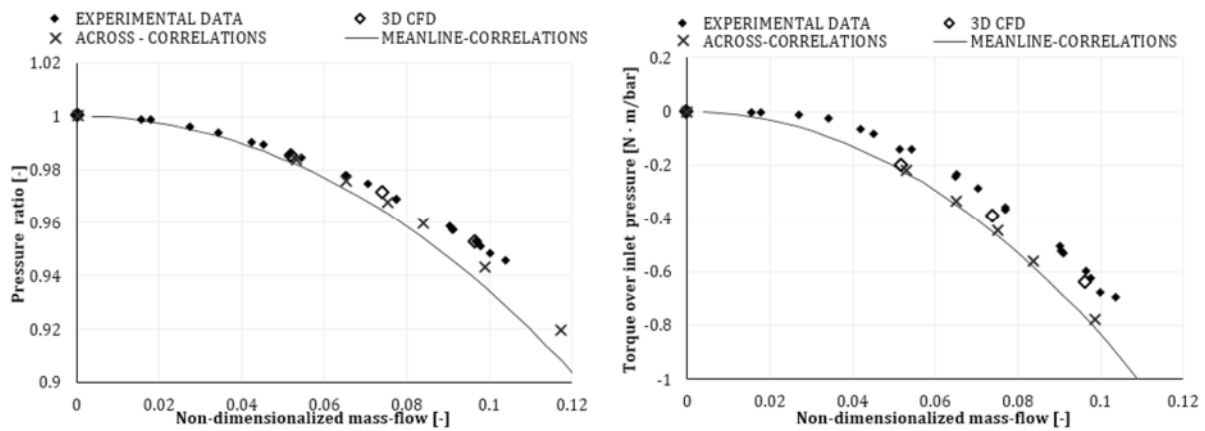


Figure 18: M250 axial compressor locked rotor characteristic calculated with different methods and compared against experiment.

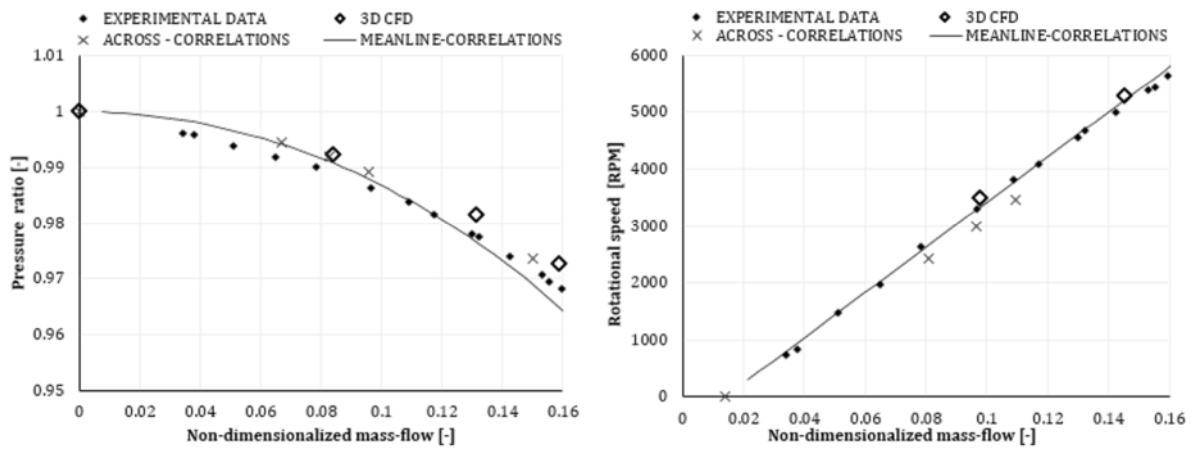


Figure 19: M250 axial compressor windmilling characteristic calculated with different methods and compared against experiment.

4. Summary and Conclusions

A model for modern compressor blades subjected to high negative incidence has been generated in terms of loss coefficient and deflection angle. The model takes solidity, stagger and incidence as inputs with an additional Mach number correction. Their application within mean-line and through-flow tools has been discussed and the usefulness in generating sub-idle compressor maps presented. In addition, the use of machine learning to fit neural networks that represent the underlying data has been shown to be a feasible candidate solution for the numerical implementation of numerical data that may not be easily described with simple analytical functions.

The model fills an existing gap in off-design blade performance information as no blade correlations spanning the full-range of negative incidences present at sub-idle conditions are known to the authors. This model may be effectively used to more accurately perform compressor off-design performance predictions using inviscid methods, such as mean-line or through-flow tools. This could allow for early prediction of compressor sub-idle performance, which is critical to ensure whole-engine ground-start and inflight relight requirements are met.

Future Work

While this model has been generated using a single blade profile, generalization to other blades may be achieved by further investigating the effects of camber and thickness on key parameters, such as the zero-lift incidence angle. Nevertheless, the current model has been applied to a wide variety of compressor blading with promising results. A number of corrections for effects such as AVDR and induced flows due to streamwise vorticity specifically targeted to high negative incidence could further improve the existing model. Additionally, the possible effects of local laminar flow on blade leading edges could be investigated with targeted tools, such as transition-modelling CFD or correlation based approaches. Finally, it is important to note that the data has been obtained entirely from numerical work. Although they have proven useful in low-order models, validation against experimental data would be required for use in more fundamental applications. This is indeed an area of future work.

Acknowledgements

The authors would like to express their gratitude to Rolls-Royce plc. for the support given to this work and for allowing its publication. The authors would also like to thank Innovate UK for funding the work. Special thanks are also due to Richard J. Tunstall for his efforts in the development of the M250 sub-idle rig. This project was also made possible by receiving funding from the Clean Sky 2 Joint Undertaking under the European Union's Horizon 2020 research and innovation programme under the grant agreement No 785349. Data subject to third party restrictions.

Nomenclature

AVDR Axial Velocity-Density Ratio

i Incidence angle [degrees]

M Mach number

MSE Mean-square error

P Pressure

PR Total pressure ratio

α	Flow angle respect to blade [degrees]
Δ	Denoting a change with respect to minimum loss conditions
δ	Deviation angle [degrees]
ϵ	Deflection angle [degrees]
γ	Stagger angle [degrees]
κ	Blade metal angle [degrees]
σ	Solidity
ω	Loss coefficient

Subscripts

0	Baseline or relating to the zero-lift condition
1,2	Fluid stations, before and after blade-row
<i>c</i>	Choking
M	Correction due to Mach number
<i>ml</i>	Minimum loss
<i>ref</i>	Reference
<i>s</i>	Denoting static conditions
<i>start</i>	Denoting cranked start
<i>t</i>	Denoting stagnation conditions
<i>wm</i>	Denoting windmilling conditions

References

- [1] Zachos, P. K., 2013, “Modelling and analysis of turbofan engines under windmilling conditions”. ASME J. Propulsion and Power, 29(4), 882–890., doi:10.2514/1.B34729
- [2] EASA, 2015, “Certification memorandum: Turbine engine relighting in flight,” Pub. L. No. CS-E 910, 1
- [3] Denton J.D.,1993,” The 1993 IGTI Scholar Lecture: Loss Mechanisms in Turbomachines,” ASME. J. Turbomach. 1993;115(4):621-656. doi:10.1115/1.2929299.
- [4] Binder N, Courty-Audren S, Duplaa S, Dufour G and Carbonneau X.,2015, “Theoretical analysis of the aerodynamics of low-speed fans in free and load-controlled windmilling operation,” ASME J. Turbomach. 2015;137(10):101001-101001-12., doi:10.1115/1.4030308.
- [5] Lieblein, S.,1960, “Incidence and deviation-angle correlations for compressor cascades,” ASME. J. Basic Eng. 1960;82(3):575-584. doi:10.1115/1.3662666.
- [6] Lieblein, S. and Roudebush, W.H. ,1956, “Theoretical loss relations for low-speed two-dimensional-cascade flow,” NACA TN-3662, Washington
- [7] Koch, C.C. and Smith, L.H.,1976, “Loss sources and magnitudes in axial-flow compressors,” Trans. of the ASME, Journal of Eng. for Power, pp. 453-462
- [8] Cetin, M., Ucer, A.S., Hirsch, Ch. and Serovy, G.K.,1987, “Application of modified loss and deviation correlations to transonic axial compressors,” AGARD-R-745, AGARD, NATO, Neuilly sur Seine, France
- [9] Howell, A.R.,1945, “Fluid dynamics of axial compressors,” Proceedins of IMechE, 153, https://doi.org/10.1243/PIME_PROC_1945_153_049_02

- [10] Carter, A.D.S.,1950, “Low-Speed Performance of Related Aerofoils in Cascade,” ARC, 29.
- [11] Creveling, H.F. and Carmody, R.H.,1968, “Computer program for calculating off-design aerodynamic performance of axial flow compressor,” NASA-CR-72427
- [12] Nocture, M., Mery, Y., Ruiz Domingo, J., Rochuon, N., Bonnal, B., Vanoli, E., Gopalakrishnan, P. and Jammalamadaka, A.,2019, “Study of high pressure compressor performances in windmilling conditions by three complementary approaches: experiment, LBM and 1D modelling,” ASME. ASME Turbo Expo 2019, GT2019-90465, Arizona, USA
- [13] Aungier, R.H.,2003, *Axial-Flow Compressors*, ASME, New York.
- [14] Roache, P.J.,1994, “Perspective: A method for uniform reporting of grid refinement studies,” Journal of Fluids Engineering, Volume 116.
- [15] Wilcox, D. C.,1993, *Turbulence modeling for CFD*, DCW Industries, Inc, La Cañada, CA.
- [16] Cumpsty N.A. and Horlock J.H.,2005, “Averaging nonuniform flow for a purpose,” ASME. J. Turbomach. 2005;128(1):120-129. doi:10.1115/1.2098807.
- [17] Greitzer, E., Tan, C., and Graf, M.,2004, *Internal Flow: Concepts and Applications (Cambridge Engine Technology Series)*, Cambridge: Cambridge University Press. doi:10.1017/CBO9780511616709
- [18] ANSYS, Inc., 2016, “ANSYS CFX Reference Guide: CFX Best Practices Guide for Turbomachinery”
- [19] Allegretti, Alessandro, 2018, “Sub-idle loss and deviation model for modern compressor blading,” MSc Thesis, Cranfield University
- [20] Meherwan P. Boyce.,2012, *Gas Turbine Engineering Handbook*. Elsevier LTD, Oxford

- [21] Illana, E., Grech, N., Zachos, P. K., and Pachidis, V., 2013, "Axial compressor aerodynamics under sub-idle conditions," ASME Turbo Expo 2013: Power for Land, Sea, and Air. San Antonio, Texas.
- [22] Schneider, Marc, 2017, "Compressor blade performance under sub-idle conditions," MSc Thesis, Cranfield University
- [23] Farokhi, S., 2014, *Aircraft Propulsion*, 2nd edition. John Wiley & Sons.
- [24] Starke, J., 1981, "The effect of the axial velocity density ratio on the aerodynamic coefficients of compressor cascades," ASME J. Engineering for Power. Vol 103, pp 210-219
- [25] Banjac, M., Petrovic, M.V., and Wiedermann, A., 2014, "A new loss and deviation model for axial compressor inlet guide vanes" ASME J. Turbomach. Volume 136.
- [26] Drela, M., 1998, "MISES implementation of modified Abu-Ghannam/Shaw transition criterion (second revision)," MIT, Cambridge, Mass.
- [27] Goodhand, M.N., 2010, "Compressor Leading Edges," PhD Thesis. University of Cambridge, Cambridge.
- [28] Lieblein, S., Robbins, R.H. and Jackson, R.J. (1965) "Blade-element flow in annular cascades," NASA SP-36, chapter VII, 1965.
- [29] Horlock, J.H., 1958, *Axial Flow Compressors: Fluid Mechanics and Thermodynamics*, Butterworths Scientific Publications, London.
- [30] Bishop, C.M., and Roach, C.M., 1992, "Fast curve fitting using neural networks," Rev. Sci. Instrum. 63, 4450; doi: 10.1063/1.1143696
- [31] Righi, M., Pachidis, M., Könözy, L. and Pawsey, M., 2018, Three-dimensional through-flow modelling of axial flow compressor rotating stall and surge, Aerospace Science and Technology, Volume 78, <https://doi.org/10.1016/j.ast.2018.04.021>.

- [32] Pollard, D., and Gostelow, J.P.,1967, “Some experiments at low speed on compressor cascades,” ASME J. Engineering for Power. July 1967, pp 437-436.
- [33] Ferrer-Vidal, L.E., Pachidis, V. and Tunstall, R.,2018, “An enhanced compressor sub-idle map generation method” Proceedings of GPPS Forum 18. Zurich, Switzerland.
- [34] Walsh, P. and Fletcher, P., 2004, *Gas Turbine Performance*, (2nd ed). Oxford, UK: Blackwell Science.
- [35] Righi, M., Ferrer-Vidal, L.E., Allegretti, A. and Pachidis, V.,2019, “Low-order models for the calculation of compressor sub-idle characteristics,” International Society for Air Breathing Engines Conference 2019, Canberra, Australia

2019-09-25

A loss and deflection model for compressor blading and high negative incidence

Ferrer-Vidal Espana-Heredia, Luis Estefano

ASME

Ferrar-Vidal LE, Schneider M, Allegretti A, Pachidis V. (2019) A loss and deflection model for compressor blading and high negative incidence. Journal of Turbomachinery, Volume 141, Issue 12, December 2019, Article number 121001, Paper number TURBO-19-1050

<https://doi.org/10.1115/1.4044967>

Downloaded from Cranfield Library Services E-Repository